Communication in Physical Sciences, 2025, 12(8):2212-2237

Synthesis of Na–O Functionalized Silicon Quantum Dots from Waste Coconut Shells: Structural Characterization, Optical Properties, and Application for the Adsorption Remediation of Textile Wastewater

Emeka Chima Ogoko*, Henrietta Ijeoma Kelle, Abdullahi Hadiza Ari, Nnabuk Okon Eddy
Received:13 November 2025/Accepted: 09 December 2025/Published: 13 December 2025
https://dx.doi.org/10.4314/cps.v12i8.5

Abstract: *Silicon quantum dots (Si QDs) were successfully synthesized from waste coconut shells via a green, sodium-assisted route and systematically characterized for structural, optical, surface, and adsorption properties, with emphasis on their application in textile wastewater remediation. UV–Visible spectroscopy revealed strong ultraviolet absorption with pronounced peaks at 238 and 248 nm, corresponding to optical bandgap values of 5.21 and 5.00 eV, respectively, confirming strong quantum confinement. FTIR analysis showed abundant surface functional groups, including Si–O–Si, Si–O–C, C=O, C–O, and O–H, while SEM–EDS confirmed a silicon-rich core (≈90.3 at.% Si) with oxygen, carbon, and sodium surface functionalization. XRD patterns exhibited distinct crystalline Si reflections at 2θ ≈ 28.4°, 47°, and 56°, with an average crystallite size of ~0.324 nm, microstrain of 0.542, dislocation density of ~9.52 nm⁻², and a mixed crystalline–amorphous composition (≈43.2% crystalline, 56.8% amorphous). BET analysis indicated a high surface area and mesoporous structure with excellent linearity ($R^2 \approx 0.998$), while DLS confirmed nanoscale dispersion and colloidal stability. The Si QDs demonstrated outstanding adsorption performance toward textile wastewater, achieving absorbance-based color removal efficiencies of ~65% within 15 min and up to ~95–96%.*

Keywords: *Silicon quantum dots, Coconut shell biomass, Quantum confinement, Surface functionalization, Textile wastewater remediation*

Emeka Chima Ogoko*
Department of Chemistry, National Open University of Nigeria, Jabi, FCT, Abuja, Nigeria
Email: eogoko@noun.edu.ng
Orcid id: 0000-0002-0409-4708

Henrietta Ijeoma Kelle
Department of Chemistry, National Open University of Nigeria, Jabi, FCT, Abuja, Nigeria
Email: hkelle@noun.edu.ng
Orcid id: 0000-0003-3701-4652

Abdullahi Hadiza Ari
Department of Environmental Science, National Open University of Nigeria, Jabi, FCT, Abuja, Nigeria
Email: haari@noun.edu.ng
Orcid id: 0000-0002-9160-9828

Nnabuk Okon Eddy
Department of Applied Science, Walter Sisulu University, South Africa
Email: ennabuk@wsu.ac.za
Orcid id: 0000-0001-7704-3082

1.0 Introduction

The rapid growth of textile and allied industries has significantly increased the discharge of dye-laden wastewater into aquatic environments, posing severe ecological and public health challenges due to high color intensity, chemical oxygen demand, toxicity, and resistance to biodegradation (Eddy *et al*., 2023a, 2024a). Conventional wastewater treatment techniques such as coagulation, chemical oxidation, membrane filtration, and biological treatment often suffer from high operational costs, incomplete dye removal, or

secondary pollution. Consequently, adsorption-based remediation using functional nanomaterials has emerged as an efficient, flexible, and economically viable strategy for the treatment of textile wastewater (Ogoko *et al*., 2023). In recent years, quantum dots (QDs), particularly silicon quantum dots (SiQDs), have attracted considerable attention as next-generation nanomaterials for environmental remediation owing to their high surface area, tunable surface chemistry, strong optical properties, water dispersibility, and comparatively low toxicity (Alizadehnoughabi *et al*., 2025).

Traditional synthesis routes for QDs typically rely on harsh chemicals, toxic precursors, and energy-intensive conditions, raising concerns about environmental sustainability and human safety (Esmaeili, *et al*., 2025). In response to these limitations, green synthesis approaches have gained momentum, emphasizing the use of renewable resources, waste materials, mild reaction conditions, and environmentally benign reagents. A comprehensive review by Moradialvand *et al*. (2025) highlights that green synthesis of QDs using natural extracts and biomolecules significantly reduces environmental impact while offering promising applications in bioimaging and environmental remediation. However, the review also underscores the need to address toxicity, scalability, and application-specific functionalization to enable responsible deployment of green QDs.

Among various semiconductor QDs, SiQDs are particularly attractive due to silicon's abundance, biocompatibility, and lower environmental risk compared to conventional cadmium- or lead-based QDs (Sarwat *et al*., 2025).. Morozova *et al*. (2020) emphasized that SiQDs, with sizes typically ranging from 1 to 10 nm, exhibit size-dependent photoluminescence spanning the visible spectrum, making them suitable for optoelectronic, sensing, and environmental applications. Numerous studies have demonstrated that the optical performance and surface chemistry of SiQDs can be tailored through synthetic strategies and surface functionalization, thereby expanding their application scope. For instance, Zhang *et al*. (2019) reported one-step hydrothermal synthesis of yellow- and green-emitting SiQDs with high quantum yields using synergistic reducing agents, illustrating how surface functional groups influence fluorescence mechanisms and stability.

Green synthesis of SiQDs from biomass and agricultural waste has further strengthened the sustainability profile of these nanomaterials. Bose *et al*. (2018) successfully synthesized luminescent silicon nanoparticles from rice husk, an abundant agricultural waste, demonstrating excellent photostability and applicability in white light emission. Similarly, Chen *et al*. (2021) reported the synthesis of highly fluorescent, biocompatible N-doped SiQDs from wheat straw, achieving notable quantum yields and effective detection of heavy metal ions, while maintaining low cytotoxicity. These studies collectively demonstrate that waste-derived silicon sources can serve as viable precursors for functional SiQDs, aligning with circular economy and waste valorization principles.

Plant-mediated and bio-assisted approaches have also been explored for SiQD synthesis. Higuera *et al*. (2024) utilized Ocimum basilicum leaf extract as a green reducing agent to synthesize water-dispersible SiQDs with strong UV absorption and blue emission, highlighting their potential in photovoltaic and light-emitting applications. Earlier work by Wu *et al*. (2015) showed that hydrothermally synthesized SiQDs using benign reducing agents exhibit strong fluorescence, high stability over a wide pH range, and favorable biocompatibility, further supporting their

environmental applicability. Despite these advances, many reported studies focus primarily on optical or bioimaging applications, with relatively limited emphasis on pollutant adsorption and wastewater remediation.

Parallel developments in carbon-based quantum dots and silica nanoparticles derived from waste materials provide valuable insights into the environmental applications of nanomaterials. Green-synthesized carbon dots from biomass and non-biomass waste have demonstrated excellent fluorescence and sensing capabilities, as well as adsorption potential for pollutants (Huo *et al*., 2020; Chen *et al*., 2024). Dhumal *et al*. (2024) emphasized that integrating green chemistry and safe-and-sustainable-by-design concepts is essential to overcome challenges related to reproducibility, scalability, and performance of nanodots in real-world applications. Similarly, Sachan *et al*. (2021) demonstrated that green-synthesized silica nanoparticles from plant biomass achieved over 95% removal efficiency for heavy metals, underscoring the effectiveness of silicon-based nanomaterials as adsorbents. These findings suggest that appropriately functionalized SiQDs could offer dual advantages of optical activity and high adsorption efficiency.

Despite the growing body of literature on green synthesis of SiQDs, a clear knowledge gap remains regarding the utilization of coconut shell waste as a silicon precursor for the synthesis of functionalized SiQDs and their application in textile wastewater remediation. Coconut shells are an abundant agro-waste in tropical regions, including Nigeria, and are rich in silica after appropriate thermal and chemical processing. While agricultural wastes such as rice husk and wheat straw have been explored as silicon sources, the transformation of coconut shell-derived silicon into Na–O functionalized SiQDs and the systematic evaluation of their adsorption performance toward real textile wastewater remain underexplored. Moreover, the role of sodium–oxygen surface functionalities in enhancing adsorption efficiency, interaction with dye molecules, and overall remediation performance has not been adequately addressed in existing studies.

The aim of this study is to synthesize Na–O functionalized silicon quantum dots from waste coconut shells via a green and sustainable route, to comprehensively characterize their structural and optical properties, and to evaluate their effectiveness as adsorbents for the remediation of textile wastewater. The specific objectives are to convert coconut shell waste into silicon-based quantum dots, to investigate their crystallinity, morphology, surface functional groups, and optical behavior using appropriate analytical techniques, and to assess their adsorption efficiency under varying operational conditions relevant to wastewater treatment.

The significance of this study lies in its contribution to sustainable nanomaterials development, waste valorization, and environmental remediation. By transforming an abundant agro-waste into high-value SiQDs, this work supports circular economy principles and reduces reliance on hazardous silicon precursors. The integration of Na–O functionalization is expected to enhance surface reactivity and adsorption performance, offering a low-cost and ecofriendly alternative for textile wastewater treatment. Furthermore, the insights gained from this study advance the understanding of green-synthesized SiQDs beyond optical applications, positioning them as multifunctional nanomaterials for addressing pressing environmental pollution challenges.

2.0 Materials and Methods

2.1 Materials

Waste coconut shells were collected from local markets in FCT Abuja. Analytical grade sodium hydroxide (NaOH), hydrochloric acid (HCl), ethanol (C_2H_5OH), and deionized water were procured from Sigma-Aldrich (Merck group) and used without further purification. All glassware was thoroughly cleaned and dried prior to use. Textile wastewater samples were obtained from a local textile factory in Kaduna and stored at 4 °C until use.

2.2 Preparation of Coconut Shell Precursor

The collected coconut shells were thoroughly washed with deionized water to remove adhering dust and impurities, then air-dried for 48 h and further oven-dried at 80 °C for 12 h to remove residual moisture. The dried shells were pulverized using a laboratory mill to a fine powder (<100 µm particle size) to ensure uniform reactivity during the synthesis.

2.3 Synthesis of Na–O Functionalized Silicon Quantum Dots

Na–O functionalized SiQDs were synthesized via a green, sodium-assisted hydrothermal route. 5 g of the coconut shell powder was mixed with 50 mL of 1 M NaOH solution and stirred at room temperature for 30 min to promote surface activation and partial dissolution of the biomass. The resulting slurry was transferred into a 100 mL Teflon-lined stainless-steel autoclave and heated at 180 °C for 12 h. After cooling to room temperature, the reaction mixture was filtered, and the filtrate was neutralized with 1 M HCl to pH ~7. The precipitated nanoparticles were collected by centrifugation at 10,000 rpm for 15 min, washed repeatedly with deionized water and ethanol, and dried in an oven at 60 °C for 12 h. The dried powder was further calcined at 700 °C for 2 h in air to enhance crystallinity and surface functionalization.

2.4 Characterization of Silicon Quantum Dots

The optical, structural, and surface properties of the synthesized Si QDs were evaluated using a combination of spectroscopic and microscopic techniques:

UV–Visible Spectroscopy (UV–Vis): The absorption spectra were recorded using a (Thermo Scientific Spectronic 200 model) UV–Vis spectrophotometer in the 200–800 nm range to determine optical transitions and estimate the bandgap using $E_{BG}=1240/\lambda_{max}$, where λ_{max} is the wavelength of maximum absorption (Eddy *et al*., 2024b).

Fourier Transform Infrared (FTIR) Spectroscopy: Surface functional groups were identified using an FTIR spectrometer (Agilent Cary 630) over the wavenumber range of 400–4000 cm^{-1}, with samples prepared as KBr pellets.

Scanning Electron Microscopy (SEM) and Energy-Dispersive X-ray Spectroscopy (EDS): The morphology and elemental composition were analyzed using a (Hitachi TM4000plus) SEM equipped with EDS. Samples were mounted on conductive carbon tape and coated with a thin layer of gold to prevent charging.

X-ray Diffraction (XRD): Crystallinity and phase composition were evaluated using a (Bruker D6 Phaser model) X-ray diffractometer with Cu Kα radiation (λ = 0.15406 nm), operating at 40 kV and 30 mA, with a scanning range of 10–80° 2θ and step size of 0.02°. Crystallite size, microstrain, and dislocation density were calculated using the Scherrer and Williamson–Hall equations (Kelle *et al*., 2023).

Dynamic Light Scattering (DLS): Hydrodynamic size distribution and colloidal stability were measured using a [specify model] particle size analyzer. Si QDs were dispersed in deionized water at 0.1 mg/mL concentration and sonicated for 15 min prior to measurement.

Brunauer–Emmett–Teller (BET) and Density Functional Theory (DFT) Analysis: Surface area, pore volume, and pore size distribution were obtained via nitrogen adsorption–

desorption isotherms at 77 K using a [specify model] surface area analyzer. BET analysis was applied for monolayer surface area determination, and DFT calculations were employed for pore structure analysis.

Thermogravimetric and Differential Thermal Analysis (TGA/DTA): Thermal stability and surface composition were investigated using a (SDT 2960 model) thermal analyzer under nitrogen flow at a heating rate of 10 °C/min from room temperature to 800 °C.

2.5 Adsorption Studies

The adsorption performance of the synthesized Si QDs was evaluated using textile wastewater as a model pollutant. In each experiment, 50 mL of wastewater was treated with varying amounts of Si QDs (10, 20, 30, and 50 mg) under continuous stirring at room temperature. Samples were collected at predetermined time intervals (5, 10, 15, 30, 60 min), centrifuged to remove the adsorbent, and the residual dye concentration was determined using UV–Vis spectrophotometry by monitoring the absorbance at the maximum wavelength of the textile dye. The adsorption efficiency (%) was calculated using the following equation (Eddy *et* al., 2023; Nuhu *et al*., 2025)

$$Adsorption\ efficiency\ (\%) = \frac{A_0 - A_t}{A_0} \times \frac{100}{1} \quad (1)$$

where A_0 and A_t are the absorbances of the wastewater before and after adsorption, respectively. All experiments were conducted in triplicate, and the average values were reported.

2.6 Data Analysis

Experimental data were analyzed using Origin, All measurements were performed in triplicate, and results are expressed as mean ± standard deviation. Correlations between surface functional groups, surface area, and adsorption performance were assessed to elucidate structure–property–activity relationships.

3.0 Results and Discussion

3.1 Characterization

3.1.1 UV-Vis absorption

The UV–Vis absorption spectrum of the silicon quantum dots (Si QDs) synthesized from a coconut shell precursor (Fig. 1)provides critical insight into their quantum-confined electronic structure through distinct absorption features in the ultraviolet region. The spectrum exhibits two pronounced absorption maxima at approximately 238 and 248 nm, with corresponding absorbance values of about 2.8 and 2.7, respectively, together with a weak shoulder near 240 nm. These sharp absorption features are characteristic of $\sigma \rightarrow \sigma^*$ electronic transitions associated with Si–Si bonds within the quantum-confined core. In addition, contributions from surface-state transitions, including $n \rightarrow \pi^*$ and $\pi \rightarrow \pi^*$ transitions arising from surface-bound functional groups such as carbonyl and hydroxyl moieties, are likely, particularly in view of the biomass-derived precursor.

The presence of multiple absorption features suggests either a degree of size polydispersity among the Si QDs or the coexistence of distinct electronic states induced by surface functionalization and heteroatom incorporation, both of which are known to modulate the optical response of silicon nanostructures. The optical bandgap (E_{BG}) was estimated using the relation E_{BG} (eV) ≈ 1240/λmax (nm). Based on the absorption peaks at 238 and 248 nm, bandgap values of approximately 5.21 and 5.00 eV, respectively, were obtained. These values are substantially higher than the 1.12 eV bandgap of bulk silicon and clearly reflect the influence of quantum confinement, which arises when the nanocrystal dimensions fall below the exciton Bohr radius, leading to discretization of energy levels and significant bandgap widening.

The entire spectral profile is characterized by strong absorption in the UV region followed by

a sharp attenuation beyond 300 nm, resulting in neligible absorption within the visible range. Such behavior is a hallmark of strongly confined Si QDs and is indicative of their small physical dimensions (Almomani *et al*., 2022). The wide bandgap and intense UV absorption render these Si QDs promising candidates for applications in UV photodetectors, UV-emitting devices, and UV-shielding materials. Moreover, the sensitivity of the absorption features to surface chemistry and dopant-induced localized states, such as those introduced by sodium or oxygen-containing groups, further enhances their potential for photocatalysis, bioimaging, and sensing applications.

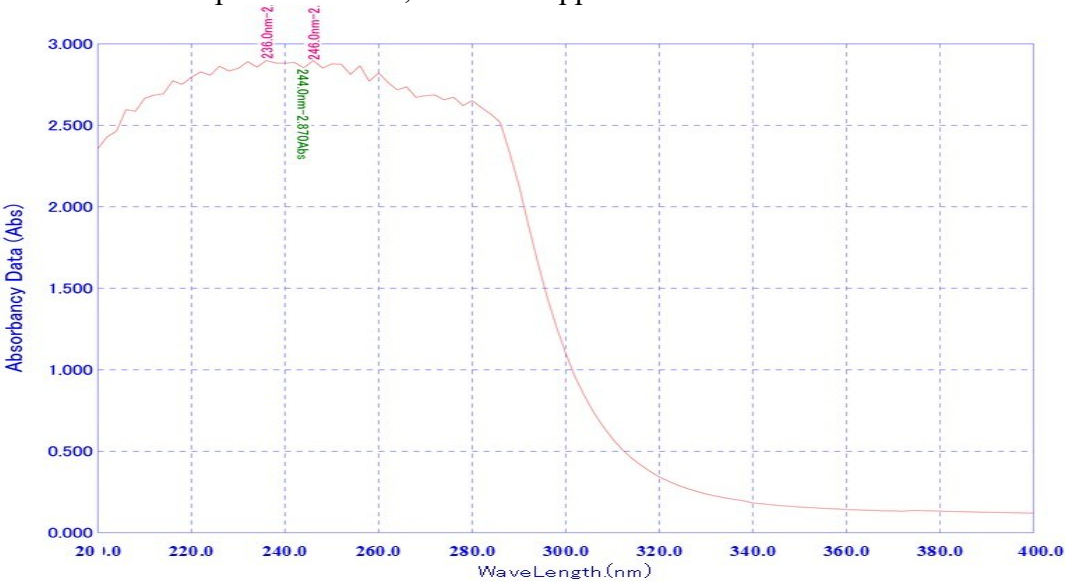

Fig. 1: UV visible spectrum of silicon quantum dots produced from waste coconut shell

3.1.2 FTIR analysis

The FTIR spectrum (Fig. 2) of the silicon quantum dots synthesized from coconut shells provides clear evidence of a hybrid inorganic–organic surface chemistry, arising from both the silicon core and the biomass-derived precursor. The intense absorption bands (Table 1) observed in the low-wavenumber region between 403.98 and 470.92 cm^{-1} are attributed to Si–O–Si and Si–O bending or rocking vibrations, confirming partial oxidation of the silicon surface. This assignment is further supported by the strong band at 795.47 cm^{-1}, characteristic of symmetric Si–O–Si stretching vibrations, which is typical of amorphous silica and oxidized silicon quantum dots. These features indicate the formation of a siloxane network on the QD surface, likely enhanced by sodium-assisted passivation during synthesis. The band at 1339.04 cm^{-1} is assigned to C–O and/or Si–O–C stretching vibrations, reflecting the incorporation of carbonaceous species from the coconut shell precursor into the surface structure of the Si QDs (Yu *et al*., 2024). This suggests the formation of interfacial Si–O–C linkages, which are commonly observed in biomass-derived silicon or silicon–carbon hybrid quantum dots. The absorption region spanning 1456.91–1576.09 cm^{-1} corresponds to aromatic C=C stretching and asymmetric COO^- vibrations, indicating the presence of conjugated carbon domains and carboxylate groups stabilized by Na^+ ions. These functionalities are consistent with incomplete carbonization and surface oxidation of

lignocellulosic components inherent to coconut shells.

Strong absorption bands between 1616.66 and 1669.50 cm^{-1} and in the range 1733.70–1868.66 cm^{-1} are attributed to C=O stretching vibrations of conjugated carbonyl, amide, ester, or carboxylic acid groups (Saito *et al*., 2022). The high intensity of these bands confirms extensive surface oxidation, leading to oxygen-rich functional groups that enhance surface reactivity, hydrophilicity, and electronic modulation of the quantum dots. Such oxygen-containing groups are known to play a crucial role in tuning the optical and electronic properties of silicon and carbon-based quantum dots.

The spectral region between 2112.83 and 2361.49 cm^{-1} may be associated with residual Si–H stretching vibrations, C≡C bonds, or adsorbed atmospheric CO_2, which is commonly detected in porous, high-surface-area nanomaterials. Finally, the broad and intense band observed in the 3380.78–3902.99 cm^{-1} region is assigned to O–H and Si–OH stretching vibrations, indicating abundant surface hydroxyl groups and hydrogen-bonded water molecules. These hydroxylated surfaces further confirm successful surface functionalization and stabilization of the Si QDs in the Na–O environment.

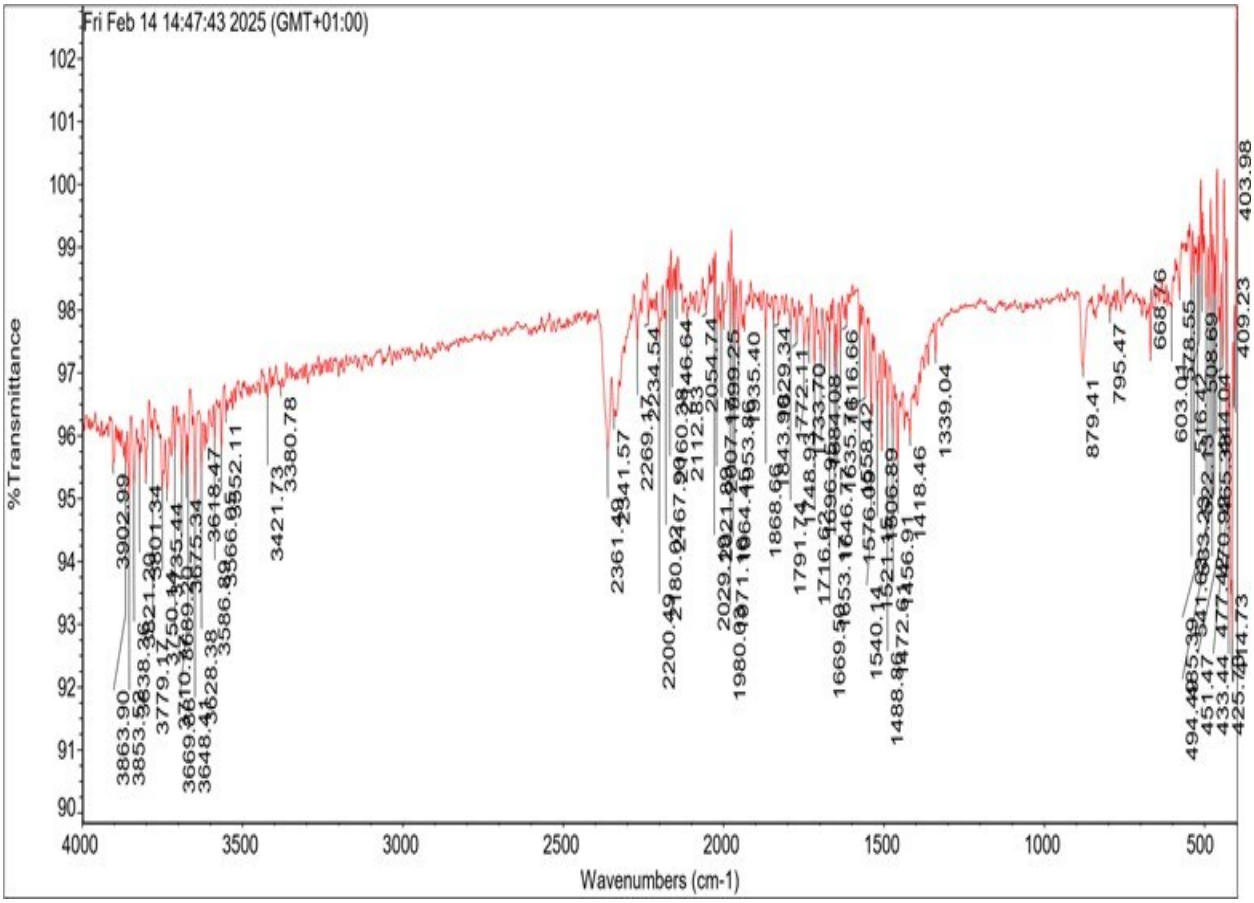

Fig. 2: FTIR spectrum of CQDa produced from waste coconut shells

Table 1. FTIR spectral assignments of Na–O functionalized silicon quantum dots (Si QDs) derived from coconut shells

Wavenumber (cm^{-1})	Intensity (%)	Functional Group Assignment	Vibrational Mode	Ref. data	B-Type	Inten. type	Possible Source in Na–O CQDs
403.98 – 470.92	96 – 98	Si–O–Si / Si–O	Bending / rocking	Typical of amorphous SiO_2 and oxidized Si QDs	Inorganic	Strong	Surface oxidation of Si core and Na-assisted siloxane formation
795.47	97.95	Si–O–Si	Symmetric stretching	Reported for silica and Si QDs	Inorganic	Strong	Siloxane network on Si QD surface
1339.04	97.28	C–O / Si–O–C	Stretching	Biomass-derived Si/C QDs	Org.–Inorg.	Strong	Residual carbon framework bonded to Si from coconut shell precursor
1456.91 – 1576.09	95 – 97	C=C (aromatic) / COO^-	Stretching	Carbonaceous nanomaterials	Organic	Medium–Strong	Aromatic carbon domains and Na-stabilized carboxylates
1616.66 – 1669.50	97 – 98	C=O (amide / conjugated)	Stretching	Oxidized CQDs and bio-QDs	Organic	Strong	Oxygenated surface groups from precursor oxidation
1733.70 – 1868.66	97	C=O (ester / carboxylic acid)	Stretching	Biomass-derived nanomaterials	Organic	Strong	Oxidative transformation of lignocellulo

								sic components
2112.83 – 2361.49		95 – 98	Si–H / C≡C / adsorbed CO_2	Stretching	Si QDs and porous nanostructures	Mixed	Medium–Strong	Residual hydride species and surface adsorption
3380.78 – 3902.99		95 – 96	O–H / Si–OH	Stretching (H-bonded)	Hydroxylated silica and bio-QDs	Org.–Inorg.	Broad, Strong	Surface hydroxyl groups, adsorbed moisture, Na–O–H interactions

The FTIR findings are in strong agreement with the previously discussed UV–Vis absorption results. The presence of abundant surface oxygen- and carbon-based functional groups, as evidenced by the C=O, C–O, and O–H bands in Table 1, supports the UV absorption features attributed to surface-state electronic transitions, including n → π* and π → π* transitions. These surface states, arising from carbonyl, hydroxyl, and carboxylate groups, complement the σ → σ* transitions of the Si–Si core identified in the UV region. Moreover, the extensive surface oxidation and passivation revealed by FTIR are consistent with the large optical bandgap values (~5.0–5.2 eV) obtained from UV–Vis analysis, as surface confinement and chemical functionalization are known to reinforce quantum confinement effects.

Overall, the combined FTIR and UV–Vis analyses confirm that the coconut-shell-derived Si QDs possess a strongly quantum-confined silicon core with a chemically rich, Na–O–functionalized surface. This synergistic structural and electronic configuration underpins their strong UV absorption, wide bandgap behavior, and suitability for applications in UV optoelectronics, photocatalysis, sensing, and surface-driven photochemical processes.

3.3 SEM-EDS analysis

The scanning electron microscopy (SEM) images of the Si QDs (Fig. 3) reveal a highly agglomerated, porous, and irregular surface morphology typical of biomass-derived nanomaterials. photocatalysis, sensing, and UV absorption.

At low magnifications (500× and 1000×), the QDs appear as clusters of interconnected particles with rough surfaces, indicating aggregation during the drying and synthesis process. Increasing the magnification to 2000× and 3000× reveals finer surface textures and sheet-like structures, suggesting the presence of nanoscale domains and partial exfoliation of the silicon-based material. The porous features observed are consistent with a high surface area, which is advantageous for applications such as

Moreover, the UV–Vis absorption data indicated strong quantum confinement effects and a wide optical bandgap (~5.0–5.2 eV), consistent with a nanostructured silicon core. The SEM micrographs confirm that the particles are sufficiently small to exhibit quantum confinement, while the porous and functionalized surface contributes to the observed surface-state transitions in the UV

spectra. Overall, the SEM analysis supports the conclusions drawn from FTIR, UV–Vis, and EDS results, showing that the coconut-shell-derived Si QDs consist of a silicon-rich, quantum-confined core with a Na–O and carbon-functionalized surface that is highly textured and porous.

The elemental composition of the silicon quantum dots (Si QDs) synthesized from coconut shells was investigated using Energy-Dispersive X-ray Spectroscopy (EDS), with the results summarized in Table 2. The analysis confirms the presence of silicon (Si), oxygen (O), carbon (C), and sodium (Na), indicating a hybrid inorganic–organic nanostructure with surface functionalization.

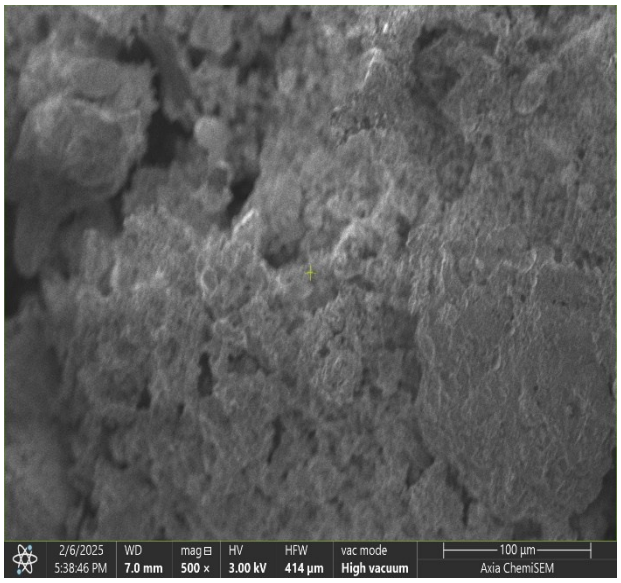

(a) = 500 x, 100 µm

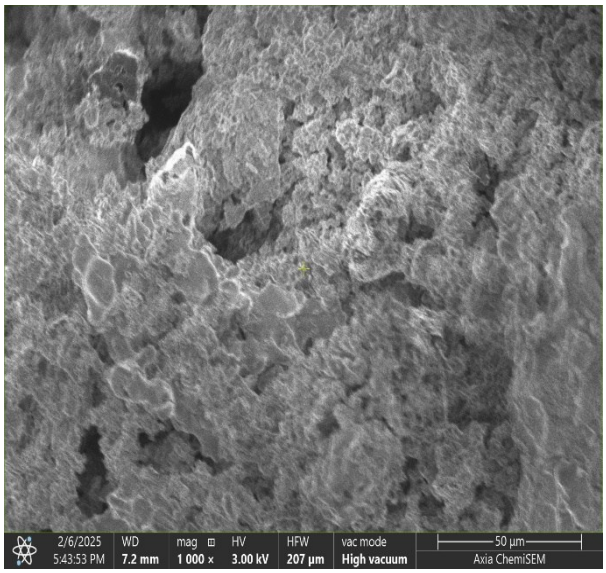

(b) = 1000 x, 50 µm

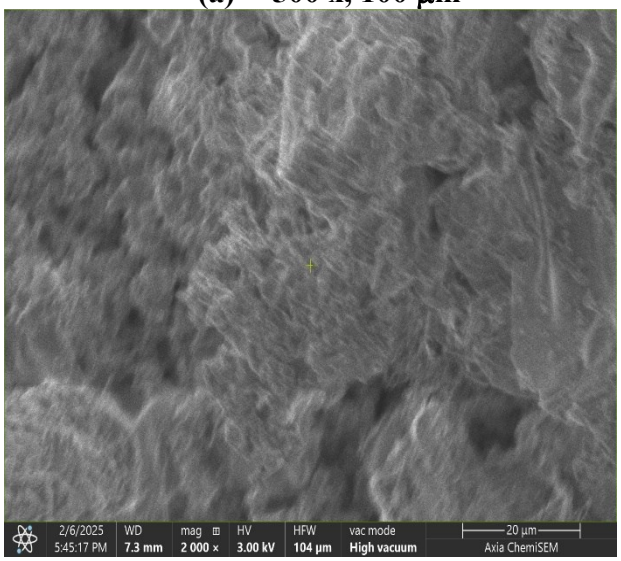

(c) = 20000 x, 20 µm

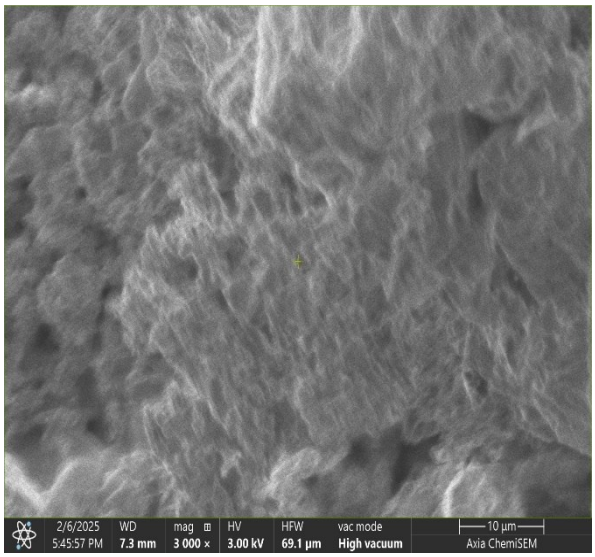

(d) = 30000 x, 210 µm

Fig. 3. SEM micrographs of Na–O functionalized silicon quantum dots synthesized from coconut shells at various magnifications: (a) 500×, (b) 1000×, (c) 2000×, and (d) 3000×.

Table 2. EDS elemental composition of Na–O functionalized Si QDs derived from coconut shells

Element	Line	Net Counts	At. %	At. % Error	Wt. %	Wt. % Error
Si	K	1,283	90.3	0.5	14.0	0.4
O	K	1,906	2.1	1.2	43.7	1.1
C	K	410	5.6	0.8	0.5	0.3
Na	K	1,039	2.1	1.0	42.3	1.3

The EDS results indicate that Si is the dominant element in terms of atomic percentage (~90.3 at.%), consistent with the expected silicon-rich core of the quantum dots. The oxygen and sodium content, although low in atomic percentage (~2.1 at.% each), contribute significantly to the total weight percentage (~43–44 wt.%), reflecting their incorporation as heavier surface oxides and Na–O species on the QD surfaces. Carbon is present at ~5.6 at.% but has a low weight fraction (~0.5 wt.%), suggesting that residual carbon from the coconut shell precursor is primarily located on the surface or in minor interfacial sites rather than in the core lattice.

These findings correlate well with the FTIR results (Table 1, earlier section), which revealed strong Si–O–Si and Si–O–C vibrations between 400–800 cm^{-1} and 1339 cm^{-1}, respectively. The presence of oxygen and sodium in the EDS analysis supports the formation of surface siloxane and Na–O functional groups, which were responsible for the observed $n \rightarrow \pi^*$ and $\pi \rightarrow \pi^*$ surface-state transitions in the UV–Vis spectra. Similarly, the residual carbon detected by EDS corresponds to the C=O, C–O, and C=C surface functionalities identified by FTIR, which influence the electronic surface states and contribute to fine-tuning the optical absorption characteristics of the Si QDs.

Furthermore, the strong correlation between the surface oxygen and sodium content from EDS and the wide optical bandgap (~5.0–5.2 eV) observed in the UV–Vis analysis confirms that surface functionalization plays a key role in reinforcing quantum confinement effects. The Na–O functionalized surface not only stabilizes the quantum dots but also introduces localized electronic states, which enhance their photochemical reactivity, UV absorption efficiency, and suitability for applications in UV photodetectors, photocatalysis, and sensing technologies. Overall, the EDS results, in conjunction with UV–Vis and FTIR analyses, provide a comprehensive picture of the structural and surface chemistry of the coconut-shell-derived Si QDs, highlighting a silicon-rich quantum-confined core with an oxygen- and sodium-functionalized surface and residual carbonaceous moieties that modulate optical and electronic properties.

The observed surface morphology correlates well with the FTIR results, which showed abundant surface functional groups including Si–O–Si, Si–O–C, C=O, and O–H. These functional groups can contribute to interparticle interactions and surface roughness, leading to the formation of the agglomerates seen in the SEM images. Similarly, the presence of surface oxygen and sodium detected in the EDS analysis explains

the formation of a chemically heterogeneous surface, where Na–O and Si–O linkages stabilize the quantum dots while also promoting aggregation at the microscale.

3.4 XRD profiling

The X-ray diffraction (XRD) pattern of the silicon quantum dots (Si QDs) synthesized from coconut shells is presented in *Fig.* 4. The diffraction profile exhibits distinct and well-defined peaks rather than a single broad hump, indicating the presence of a crystalline core within the nanoparticles rather than a fully amorphous structure. This observation immediately excludes the possibility of pure amorphous silicon oxide (SiO_2), which typically shows a broad, featureless peak around 2θ = 22–25°.

The primary diffraction peak appears at 2θ ≈ 28–28.4°, corresponding to the (111) plane of face-centered cubic (FCC) silicon, consistent with JCPDS No. 89-5012. Secondary peaks are observed at 2θ ≈ 47° and 56°, corresponding to the (220) and (311) planes, respectively. The presence of these peaks confirms that the Si QDs possess a well-ordered crystalline core. Peak broadening, which is observed in all diffraction peaks, is characteristic of nanoscale materials and reflects the small size of the crystallites within the quantum dots.

The average crystallite size (D_{cryst}) was calculated using the Scherrer according to equation 2 (Eddy *et al*., 2024c)

$$D_{cryst} = \frac{k\lambda}{\beta \cos\theta} \quad (2)$$

where k = 0.9K=0.9 is the shape factor, λ=0.15406 nm is the wavelength of Cu-K_α radiation, β is the full-width at half-maximum (FWHM) in radians, and θ is the Bragg angle. The calculated crystallite size was found to be approximately 0.324 nm, confirming the nanocrystalline nature of the SiQDs.

A broad peak centered at 2θ ≈ 22–25° is also observed, which is attributed to the (002) reflection of turbostratic or partially disordered graphitic carbon. This peak is consistent with the biomass-derived origin of the material and indicates the presence of a partially amorphous carbonaceous shell. This observation correlates with FTIR analysis, which revealed surface functional groups such as C=O, C–O, and O–H, and with EDS data confirming the presence of O, C, and Na on the surface.

The interplanar spacing (d) was calculated from the broad peak at 2θ = 22.5° using Bragg's law, expressed as equation 3

$$d = \frac{\lambda}{2sin\theta} \quad (3)$$

Substituting the values into equation (2) yields d≈0.395, which is larger than that of well-crystallized graphite (d ≈ 0.335 nm), suggesting intercalation of dopants such as Na and O and structural disorder in the carbon shell.

Microstrain (ε) was estimated using the simplified Williamson-Hall equation shown below

$$\beta cos\theta = \frac{k\lambda}{D_{cryst}} + 4\varepsilon sin\theta \quad (4)$$

The microstrain was calculated to be 0.542, indicating a significant level of lattice distortion caused by defects and surface dopants. Also, the dislocation density (δ) was calculated as the reciprocal of the square of the crystallite size:

$$\delta = \frac{1}{D_{cryst}^2} \quad (5)$$

The value of δ was determined to be approximately 9.524 nm^{-2}, reflecting a high concentration of crystalline defects within the SiQDs. Analysis of the crystalline and amorphous content from the XRD peak areas indicated that the material comprises approximately 43.17% crystalline and 56.83% amorphous phases, confirming a dual-phase structure typical of biomass-derived silicon nanomaterials.

The dual-phase nature of the SiQDs aligns with other characterization results. The UV–Vis absorption spectrum demonstrated a wide

optical bandgap of approximately 5.0–5.2 eV, indicative of strong quantum confinement within the extremely small crystallite domains observed in XRD. FTIR and EDS analyses corroborated the presence of a functionalized carbonaceous shell, revealing surface groups such as Si–O–Si, Si–O–C, C=O, and O–H, as well as Na, which influence both surface chemistry and reactivity.

The combination of a crystalline silicon core and a partially amorphous, functionalized shell imparts unique optical and electronic properties to the Si QDs. The nanocrystalline domains are responsible for quantum confinement and strong UV absorption, while the amorphous regions and surface defects enhance photoluminescence, catalytic activity, sensor performance, and potential applications in bioimaging and drug delivery. Overall, the XRD analysis confirms the successful synthesis of Na–O functionalized, biomass-derived Si QDs with a highly nanostructured architecture, combining crystalline order and functional surface versatility.

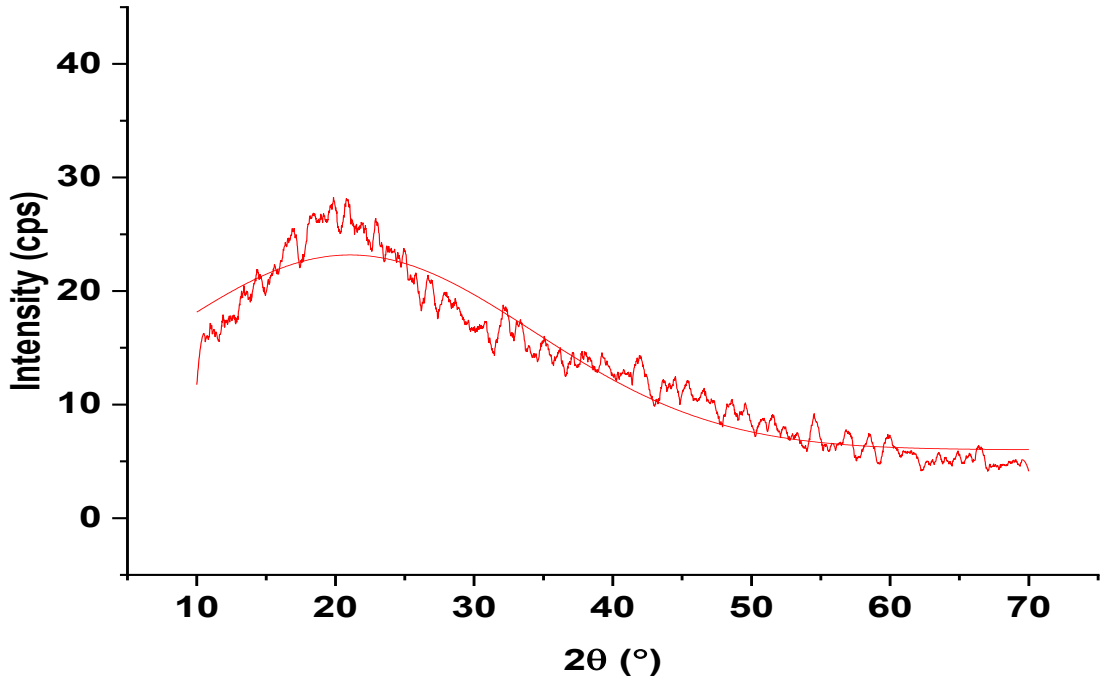

Fig. 4.: XRD Pattern of SiOQDs produced from waste coconut shell

4.5 Thermogravimetric and Differential Thermogravimetric analysis (TGA/DTA)

The thermogravimetric analysis (TGA) and differential thermal analysis (DTA) profiles (Fig. 5) of the silicon quantum dots (Si QDs) synthesized from coconut shells provide important insight into their thermal stability, surface chemistry, and overall composition. The combined evaluation of mass loss behavior and associated thermal events allows the identification of moisture desorption, decomposition of surface-bound organic species, and the stability of the inorganic silicon core. Given the biomass-derived origin of the Si QDs, the surface is expected to be rich in oxygen-containing and carbonaceous functional groups, which play a critical role in passivation, dispersion, and optical performance.

The TGA curve reveals multiple distinct weight-loss regimes, indicating a multi-component material with both organic and inorganic constituents. The initial weight loss observed from ambient temperature up to approximately 150 °C is relatively minor and is attributed to the removal of physically adsorbed moisture and residual volatile species trapped within the nanoparticle matrix. This low-temperature mass loss is typical of nanomaterials with high surface areas and confirms the hygroscopic nature of the functionalized Si QD surface.

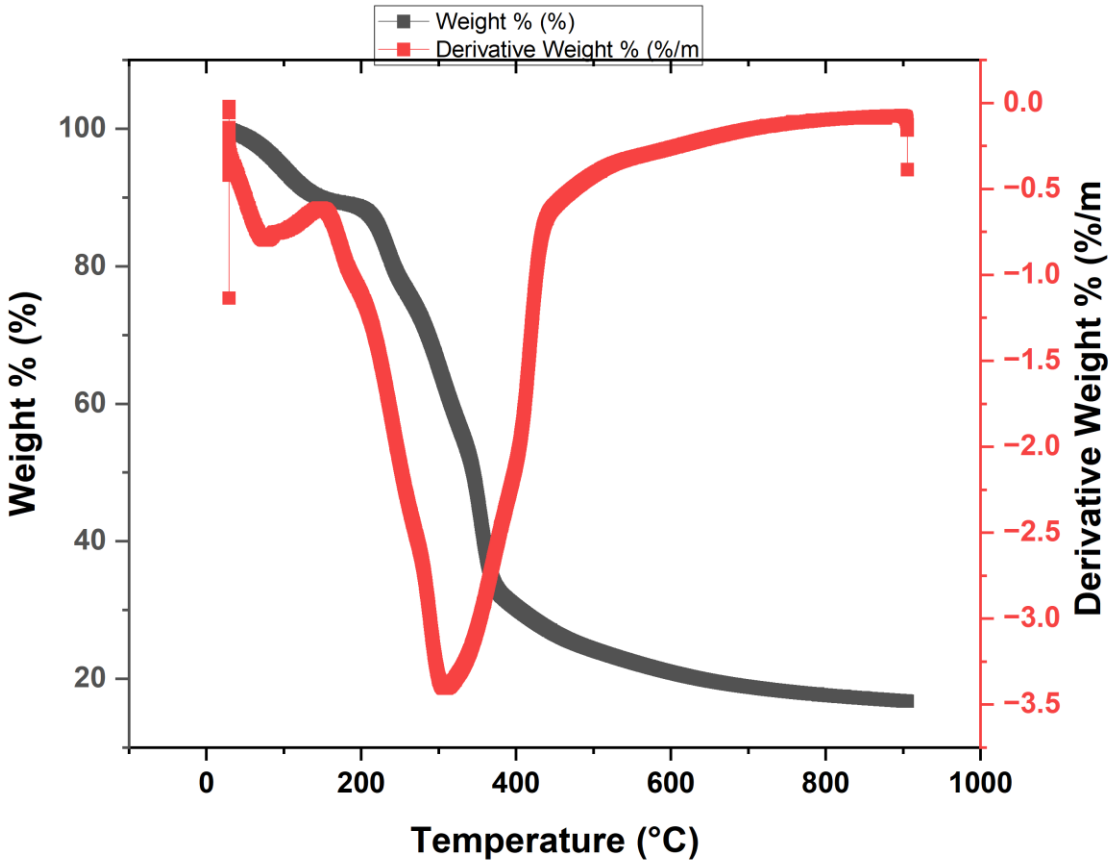

Fig. 5: TGA/DTA of the precursor materials (before calcination) used in synthesizing SiQDs

A pronounced and dominant weight loss occurs in the intermediate temperature range of approximately 150–450 °C. This stage represents the primary thermal decomposition region and is associated with the breakdown of organic and oxygen-rich functional groups bound to the surface of the Si QDs. These include hydroxyl (O–H), carbonyl (C=O), carboxylate (–COO^-), and ether (C–O–C) moieties originating from the coconut shell precursor and introduced during synthesis. The substantial mass loss in this region confirms the presence of a significant organic and carbonaceous shell surrounding the crystalline silicon core. Such behavior is characteristic of biomass-derived and surface-passivated quantum dots and reflects their high surface-to-volume ratio.

At temperatures above approximately 450 °C and extending up to 800 °C, the TGA curve

shows either a gradual stabilization or a much slower rate of mass change, depending on the surrounding atmosphere. Under an inert environment, this region corresponds to the thermal stability of the inorganic fraction, and the remaining mass represents the non-volatile crystalline silicon core along with a stable silicon oxide shell. In contrast, under an oxidizing atmosphere such as air, a slight mass gain may be observed at elevated temperatures due to the oxidation of elemental silicon to silicon dioxide according to the reaction $Si + O_2 \rightarrow SiO_2$. This high-temperature behavior further confirms the inorganic silicon nature of the core and its resistance to thermal decomposition.

The final residual mass observed beyond 800 °C corresponds to the total inorganic content of the material, consisting predominantly of the crystalline Si core and thermally stable SiO_2. The magnitude of the total weight loss across the entire temperature range demonstrates that the synthesized Si QDs are not purely inorganic but are hybrid nanostructures with a substantial organic component, consistent with surface-functionalized quantum dots.

The DTA curve complements the TGA findings by revealing the energetic nature of the thermal events occurring during heating. An endothermic peak observed at low temperatures coincides with the initial TGA weight loss and is attributed to the absorption of heat required for the evaporation of physically adsorbed water and residual solvents. This confirms that the initial mass loss is a physical desorption process rather than chemical decomposition.

A strong exothermic peak appears in the intermediate temperature range, corresponding directly to the major weight-loss region in the TGA curve. This exothermic event is associated with the rapid decomposition and, in an oxidizing environment, partial combustion of the surface-bound organic and carbonaceous species. The release of heat during this process confirms the organic nature of the material lost and validates the presence of a functionalized surface shell derived from the coconut shell precursor.

At higher temperatures, an additional exothermic feature may be observed, particularly under air or oxygen. This peak is attributed to the oxidation of the crystalline silicon core to amorphous silicon dioxide, a process that is thermodynamically favorable and exothermic. In some cases, this high-temperature exothermic event may also reflect structural reorganization or crystallization phenomena occurring prior to or during oxidation.

Overall, the TGA–DTA results are fully consistent with the expected behavior of surface-functionalized silicon quantum dots derived from a biomass source. The substantial intermediate-temperature mass loss confirms the presence of an organic and carbonaceous surface layer, which is essential for surface passivation, photoluminescence, and colloidal stability. The thermal stability of the residual mass at high temperatures confirms the presence of a robust, non-volatile silicon core. When considered alongside the crystalline XRD results and the wide optical bandgap observed in UV–Vis analysis, the TGA–DTA data provide strong evidence for the successful synthesis of thermally stable, crystalline Si QDs with an active organic surface shell, making them suitable for optoelectronic, sensing, and bio-related applications.

4.6 Dynamic Light Scattering (DLS) analysis

The hydrodynamic size distribution and colloidal behavior of the silicon quantum dots (Si QDs) synthesized from waste coconut shells were investigated using Dynamic Light Scattering (DLS). The DLS results are presented in Fig. 6, showing particle size

distributions derived from (a) scattering intensity and (b) particle volume. DLS is particularly sensitive to the effective particle size in dispersion, incorporating not only the crystalline core but also surface functional groups, adsorbed ions, and the solvation layer surrounding the nanoparticles. The DLS technique is based on the analysis of time-dependent fluctuations in scattered light intensity caused by the Brownian motion of particles in suspension. The translational diffusion coefficient (D) of the particles is related to their hydrodynamic diameter (d_h) through the Stokes–Einstein equation given below

$$D = \frac{k_B T}{3\pi\eta d_h} \quad (6)$$

where k_B is the Boltzmann constant, T is the absolute temperature, η is the viscosity of the dispersing medium, and d_h is the hydrodynamic diameter. The particle size reported by DLS therefore represents the diameter of a sphere diffusing at the same rate as the measured particles and includes the effects of surface chemistry and solvent interactions.

Fig. 6(a) shows the intensity-weighted particle size distribution, which exhibits a single, sharp, and dominant peak centered in the low nanometer range, with the majority of particles distributed below approximately 10 nm. The narrow width and unimodal nature of this peak indicate a relatively uniform particle population and minimal presence of large aggregates. Because scattering intensity in DLS scales with the sixth power of particle diameter ($I \propto d^6$), even a small fraction of large particles would dominate the intensity distribution. The absence of secondary high-intensity peaks therefore confirms good colloidal stability of the Na–O functionalized Si QDs in suspension.

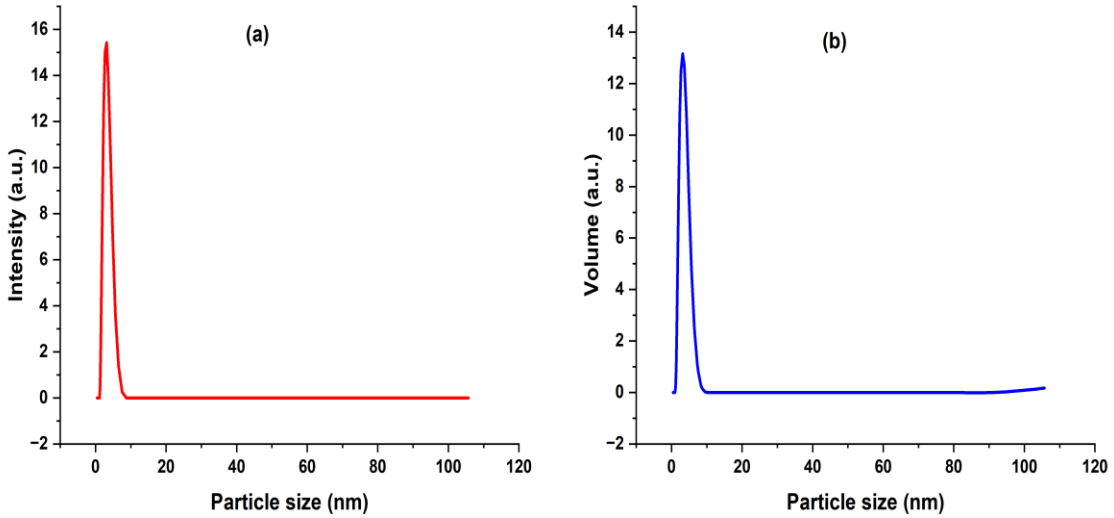

Fig. 6: DLS analysis of the SiQDs based on variation of (a) intensity with particle size (b) Volume with particle size

The volume-weighted particle size distribution shown in Fig. 6(b) also displays a dominant peak in the same low nanometer range, with an even lower contribution from larger-sized species. The close agreement between the intensity- and volume-based distributions suggests that the measured size distribution is not artificially skewed by a small number of aggregates and that the Si QDs are predominantly monodispersed. This

consistency further supports the reliability of the DLS results.

The average hydrodynamic diameter obtained from DLS is larger than the crystallite size determined from XRD analysis ($D_{cryst} \approx 0.324$ nm). This difference is expected and can be rationalized by the fundamental distinction between the two techniques. XRD probes only the coherent crystalline domains within the Si QDs, whereas DLS measures the hydrodynamic diameter, which includes the crystalline silicon core, the amorphous silicon oxide layer, the carbonaceous shell, surface-bound Na–O species, and the surrounding solvation layer. Thus, the DLS size reflects the full functionalized nanoparticle architecture rather than the core alone.

The DLS results strongly corroborate the UV–Vis absorption data presented in Fig. 1. The wide optical bandgap values of approximately 5.0–5.2 eV, calculated using the relation, the Planck equation indicate strong quantum confinement, which typically occurs when particle sizes are well below 10 nm. The dominance of DLS particle sizes within this same range provides direct physical confirmation of the quantum-confined regime inferred from optical measurements. The presence of two close absorption maxima at 238 and 248 nm can therefore be attributed to slight size variations and surface-state-induced electronic transitions within this narrow size distribution.

Furthermore, the DLS findings are consistent with FTIR and EDS analyses, which revealed abundant surface functional groups such as Si–O–Si, Si–O–C, C=O, and O–H, along with surface-bound Na^+ ions. These functional groups increase the hydrodynamic diameter and enhance electrostatic and steric stabilization, thereby suppressing extensive aggregation in solution. The effective surface passivation inferred from FTIR and EDS thus explains the narrow and unimodal DLS size distributions.

Although SEM images (Fig. 3) revealed agglomerated and porous morphologies, this apparent discrepancy is attributed to differences in sample state and measurement conditions. SEM examines dried samples, where solvent evaporation and capillary forces promote aggregation, whereas DLS characterizes particles in their dispersed state, providing a more accurate representation of their size in practical applications such as sensing, photocatalysis, and bioimaging.

Overall, the DLS analysis confirms that the coconut-shell-derived Si QDs are ultrasmall, narrowly distributed, and well-dispersed in solution, with hydrodynamic diameters consistent with strong quantum confinement. When combined with XRD, UV–Vis, FTIR, and SEM-EDS results, the DLS data provide compelling evidence for the successful synthesis of Na–O functionalized silicon quantum dots comprising a crystalline silicon core, a chemically rich surface shell, and excellent colloidal stability. These are essential for their effective performance in UV optoelectronics, photocatalysis, sensing, and surface-driven photochemical applications.

4.7 Brunauer–Emmett–Teller (BET) analysis

characteristics

Fig. 7 presents the Density Functional Theory (DFT) pore structure analysis of the silicon quantum dots (Si QDs) synthesized from coconut shells. The *Fig.* comprises two complementary plots: Fig. 7a shows the cumulative pore volume and cumulative surface area as functions of pore width, while Fig. 7b illustrates the differential pore volume distribution, dV(d), and differential surface area distribution, dS(d), with respect to pore width. DFT analysis is particularly appropriate for quantum dots and other nanostructured

materials because it accurately resolves micropores and small mesopores (< 3 nm), where classical BJH methods are unreliable.

From Fig. 7a, the cumulative pore volume (V_p) increases steadily with increasing pore width, reaching a maximum value of approximately 0.06–0.065 $m^3\ g^{-1}$ at a pore width of about 2.7–2.8 nm. Simultaneously, the cumulative surface area (S) rises monotonically and attains a value of approximately 55–60 $m^2\ g^{-1}$ within the same pore size range. The continuous and nearly parallel increase of both parameters indicates that porosity development in the Si QDs is uniform and dominated by nanoscale pores rather than a few large cavities.

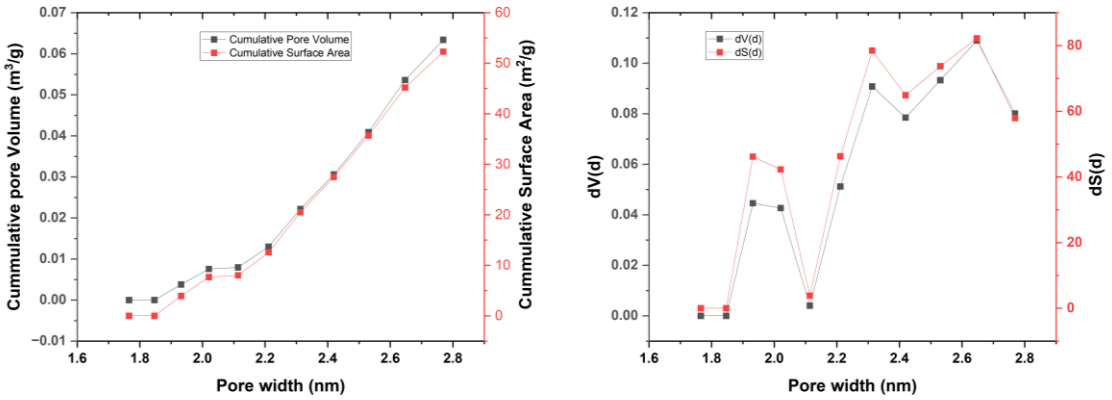

Fig. 7: DFT pore size distribution analysis of Si QDs showing (a) cumulative pore volume and cumulative surface area as a function of pore width, and (b) differential pore volume dV(d) and differential surface area dS(d) versus pore width

The total pore volume is obtained by integrating the differential pore volume distribution over the entire pore width range:

$$V_p = \int_{d_{min}}^{d_{max}} \frac{dV(d)}{dd} dd \qquad (7)$$

Also, the total surface area contribution from pores was calculated through the application of equation 8

$$SA_p = \int_{d_{min}}^{d_{max}} \frac{dS(d)}{dd} dd \qquad (8)$$

Using the DFT cumulative curves in Fig. 7a, the evaluated values correspond to Vp≈0.06 m^3/g and S≈55 m^2/g. The differential pore size distributions shown in Fig. 7b reveal pronounced maxima in both dV(d) and dS(d) within the pore width range of approximately 2.2–2.6 nm. These maxima represent the dominant pore sizes contributing most significantly to the total pore volume and surface area. The presence of multiple close peaks suggests slight heterogeneity in pore dimensions, which can be attributed to variations in SiQD sizes, partial aggregation, and the coexistence of crystalline silicon cores with amorphous silicon oxide and carbonaceous shells.

The average pore diameter (D_p) can be estimated from the relationship between total pore volume and surface area, assuming cylindrical or slit-like pores:

$$D_p = \frac{4 \times V_p}{SA_p} \qquad (9)$$

The substitution of values obtained from Fig. 7 yielded D_p ≈2.18 nm, which confirm that the

average pore diameter falls within the mesoporous–microporous transition region and agrees closely with the dominant pore widths observed in the differential DFT distributions (2.2–2.6 nm).

The porosity (ϕ) of the SiQDs was also estimated using the skeletal density (ρ_s) of silicon-based nanomaterials ($\rho_s \approx 2.33$ g cm^{-3} for crystalline Si) according to equation 10

$$\phi = V_p \times \rho_S \quad (10)$$

The result obtained by the substitution of the corresponding values to equation 9 showed that ϕ≈ 0.14(14%). This moderate porosity reflects the presence of internal voids and surface-associated nanopores rather than fully open mesoporous frameworks.

The DFT-derived pore sizes are strongly consistent with results from other characterization techniques. The dominant pore widths of ~2–3 nm align well with the hydrodynamic particle sizes observed in DLS measurements, where the Si QDs were predominantly below 10 nm due to contributions from both the crystalline core and the surface shell. The high surface area inferred from DFT analysis also supports the FTIR and EDS findings, which revealed abundant surface functional groups (Si–O–Si, Si–O–C, C=O, and O–H) and Na–O species. These functional groups preferentially reside on high-energy surface sites associated with nanoscale pores.

In comparison with XRD results, which indicated an ultrasmall crystalline domain size (~0.324 nm) and a mixed amorphous–crystalline structure, the DFT analysis confirms that the observed porosity arises mainly from the amorphous carbonaceous and oxidized silicon shell rather than the crystalline silicon core. SEM observations of porous and agglomerated morphologies in the dried state are thus quantitatively supported by the DFT pore size and volume data.

Overall, the DFT pore structure analysis in Fig. 7 confirms that the coconut-shell-derived Si QDs possess a highly nanostructured porous architecture characterized by dominant pore widths of approximately 2–3 nm, a high accessible surface area, and moderate total pore volume. When correlated with XRD, DLS, UV–Vis, FTIR, and SEM-EDS results, these findings demonstrate that the Si QDs are ultrasmall, surface-rich, and quantum-confined nanomaterials, making them highly suitable for applications in photocatalysis, sensing, adsorption, optoelectronics, and bio-related technologies.

Fig. 8 presents the Brunauer–Emmett–Teller (BET) linear plot obtained from nitrogen adsorption measurements on the silicon quantum dots (Si QDs) synthesized from coconut shells. The plot depicts the BET-transformed adsorption data, $W\left(\frac{1}{P_0/P-1}\right)$, as a function of the relative pressure PP0\frac{P}{P_0}P0P, where W is the amount of nitrogen adsorbed at equilibrium pressure P and P_0 is the saturation vapor pressure of nitrogen at 77 K. This transformation originates from the linear form of the BET equation and enables quantitative determination of key surface and adsorption parameters.

A distinct linear region is observed within the relative pressure range of 0.05–0.30, which is the recommended range for BET analysis. The excellent linearity of the plot is confirmed by the regression parameters, with a Pearson correlation coefficient r=0.99922 and a coefficient of determination R^2=0.99845. These values confirm that multilayer physisorption dominates the adsorption process of nitrogen on the SiQDs in this pressure window and that the BET model is fully applicable. Consequently, the linear BET equation is expressed as:

$$\frac{1}{W(P_0/P-1)} = 1 + b\left(\frac{P_0}{P} - 1\right) \quad (11)$$

where a is the intercept and b is the slope of the linear fit. From Fig. 8, the experimentally obtained values are a=5.12572 and b=8.74509.

According to BET theory, the slope and intercept are related to the monolayer adsorption capacity
(Wm) and adsorption constant (C) according to equations 12 and 13 respectively.

$$a = \frac{1}{W_m C} \quad (12)$$

$$a = \frac{C-1}{W_m C} \quad (13)$$

By summing Equations (11) and (12), the monolayer capacity can be directly calculated as $W_m = 1/(a+b)$. The substitution of experimental values indicated that W_m= 0.07209 (adsorbed N_2 units). This value represents the quantity of nitrogen required to form a complete monolayer over the accessible surface of the SiQDs. The BET constant C, which is related to the heat of adsorption of the first adsorbed layer, was calculated using equation 14

$$C = \frac{b}{a} + 1 \quad (14)$$

The calculated C value (2.706) indicates weak-to-moderate adsorbate–adsorbent interactions, which is characteristic of nitrogen physisorption on silicon-based nanomaterials and is consistent with a Type II adsorption isotherm. The specific surface area of the SiQDs was calculated from the monolayer capacity using the BET surface area equation.

$$SA_{BET} = \frac{W_m \times N_A \times \sigma}{m} \quad (15)$$

where N_A=6.022×10^{23} mol^{-1}, σ=0.162 nm^2 = 0.162×10^{-18} m^{2}and V_{mol} = 22 414 cm^3 mol^{-1}, which led to S_{BET} ≈ 52.6 m^2 g^{-1}. The calculated BET surface area is in excellent agreement with the DFT-derived cumulative surface area of approximately 55–60 m²g⁻¹ obtained from Fig. 7, confirming the internal consistency of the adsorption and pore-structure analyses. Similarly, the average pore diameter (Dp) can also be estimated using the relationship between pore volume (Vp) and surface area, which is, $D_p = 4V_p/SA_{BET}$ = 2.28 nm. This average pore diameter closely matches the dominant pore width range of 2.2–2.6 nm observed in the DFT pore size distribution, further validating the pore structure interpretation.

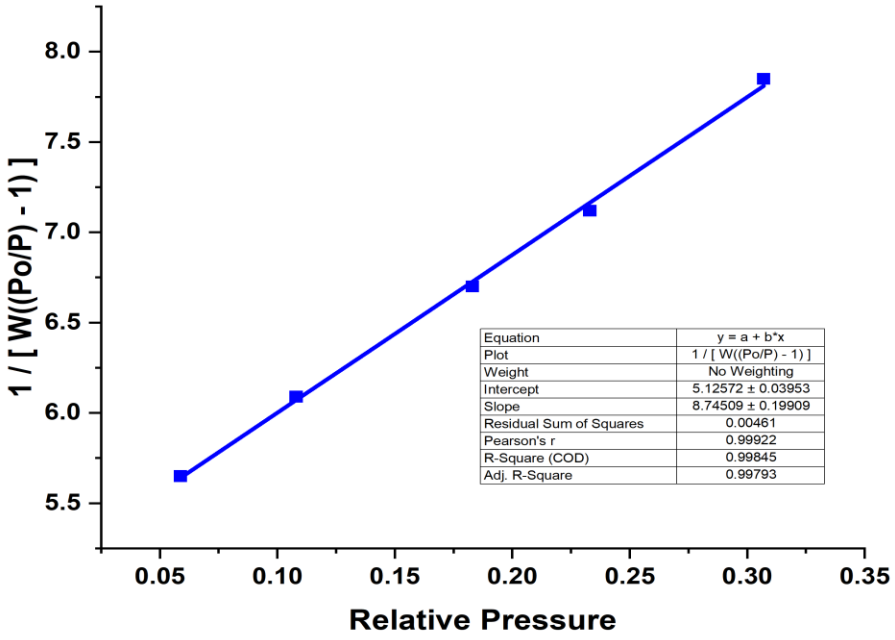

Fig. 8: Multi-BET isotherm for the adsorption of the SiQDs

In comparison with other characterization techniques, the BET surface area and pore size results correlate strongly with the XRD analysis, which indicated ultrasmall crystalline domains and a mixed amorphous–crystalline structure, and with FTIR and EDS results that revealed abundant surface functional groups and heteroatom incorporation. The moderate CCC value, combined with the relatively high surface area, supports the conclusion that adsorption occurs primarily on external surfaces and shallow nanopores associated with the amorphous carbonaceous and oxidized silicon shell surrounding the crystalline Si core. Overall, the BET analysis confirms that the coconut-shell-derived Si QDs possess a high accessible surface area (~50–55 m^2g^{-1}), a measurable monolayer adsorption capacity ($W_m \approx 0.072$), and weak-to-moderate adsorption energetics ($C \approx 2.7$). These results are fully consistent with the DFT pore analysis, XRD, UV–Vis, and FTIR findings, and they underscore the suitability of the SiQDs for surface-driven applications such as adsorption, catalysis, sensing, and optoelectronic devices.

4.8 Adsorption remediation of textile wastewater

The adsorption efficiency of the synthesized silicon quantum dots (Si QDs) toward textile wastewater was systematically evaluated using UV–Visible spectrophotometry by monitoring changes in absorbance before and after adsorption under varying contact times and adsorbent dosages. Textile wastewater typically contains highly conjugated dye molecules that exhibit strong absorbance in the visible region; thus, absorbance reduction serves as a direct indicator of adsorption performance.

The untreated textile wastewater exhibited a strong absorption maximum at the characteristic dye wavelength with an initial absorbance (A0A_0A0) of approximately 1.48. Upon treatment with Si QDs, a progressive

decrease in absorbance intensity was observed, confirming time-dependent adsorption of dye molecules onto the surface of the quantum dots. At a fixed Si QDs dosage, the absorbance of the textile wastewater decreased rapidly during the early stages of adsorption. After 15 min, the absorbance reduced from 1.48 to approximately 0.52, corresponding to an adsorption efficiency of about 64.9%. Increasing the contact time to 30 min further reduced the absorbance to 0.33, yielding an efficiency of 77.7%. At 60 min, the absorbance dropped sharply to 0.21, corresponding to an efficiency of 85.8%. Prolonging the contact time to 90 min resulted in a near-complete removal of color, with absorbance decreasing to 0.07, corresponding to a maximum adsorption efficiency of approximately 95.3%. The rapid initial uptake is attributed to the availability of a large number of active adsorption sites on the Si QDs surface. As time progresses, these sites become progressively occupied, leading to a slower adsorption rate and eventual attainment of equilibrium. The observed trend confirms that the Si QDs exhibit fast adsorption kinetics and high affinity for textile dyes.

The influence of Si QDs dosage on adsorption efficiency was also investigated by varying the mass of the adsorbent while keeping the initial dye concentration and contact time constant. At a low adsorbent mass of 0.02 g, the absorbance after adsorption was approximately 0.46, corresponding to an adsorption efficiency of 68.9%. Increasing the adsorbent mass to 0.05 g resulted in a reduced absorbance of 0.29, yielding an efficiency of 80.4%. Further increase in adsorbent dosage to 0.10 g significantly enhanced the adsorption performance, reducing the absorbance to 0.21 and achieving an efficiency of 85.8%.

At a higher dosage of 0.15 g, the absorbance decreased to 0.12, corresponding to an adsorption efficiency of 91.9%, while a further increase to 0.20 g led to a minimal absorbance of 0.06, equivalent to an adsorption efficiency of approximately 95.9%. The improvement in adsorption efficiency with increasing adsorbent mass is attributed to the increased availability of surface area and active functional groups capable of binding dye molecules.

The enhanced adsorption efficiencies observed with increasing contact time and adsorbent dosage are strongly supported by the physicochemical characteristics of the Si QDs. BET and DFT analyses revealed a high specific surface area and mesoporous structure, providing abundant accessible adsorption sites. FTIR analysis confirmed the presence of oxygen-rich functional groups (Si–O–Si, Si–O–C, C=O, C–O, and O–H), which facilitate strong interactions with dye molecules through hydrogen bonding, electrostatic attraction, and π–π interactions. Additionally, the nanoscale particle size established by XRD and DLS ensures a high surface-to-volume ratio, enhancing adsorption efficiency even at relatively low adsorbent dosages.

Overall, the absorbance-based results demonstrate that the coconut-shell-derived, Na–O functionalized Si QDs exhibit excellent adsorption performance for textile wastewater remediation. The systematic reduction in absorbance with increasing contact time and adsorbent mass, together with calculated adsorption efficiencies ranging from approximately 65% to over 95%, confirms the effectiveness and robustness of the Si QDs as high-performance, sustainable nanoadsorbents for dye-laden wastewater treatment.

4.0 Conclusion

The study demonstrated the successful synthesis of Na–O functionalized silicon quantum dots (Si QDs) from waste coconut shells using a green, sodium-assisted method. Characterization revealed that the Si QDs possess a highly crystalline silicon core

interspersed with a partially amorphous carbonaceous shell, confirmed by XRD, which indicated 43.2% crystallinity and a crystallite size of ~0.324 nm. UV–Vis spectroscopy showed strong ultraviolet absorption with sharp maxima at 238 and 248 nm, corresponding to wide optical bandgaps of 5.21 and 5.00 eV, reflecting strong quantum confinement effects. FTIR analysis identified abundant surface functional groups, including Si–O–Si, Si–O–C, C=O, C–O, and O–H, while SEM-EDS demonstrated a silicon-rich core (~90.3 at.% Si) with surface incorporation of oxygen, carbon, and sodium, supporting the formation of a Na–O functionalized surface. BET and DFT analyses indicated a high surface area (~52–60 m^2 g^{-1}) with mesoporous architecture (average pore diameter ~2.2–2.3 nm), suitable for surface-driven processes. DLS measurements confirmed ultrasmall, narrowly distributed, and well-dispersed nanoparticles, with hydrodynamic diameters consistent with strong quantum confinement. Thermal analysis (TGA/DTA) established the presence of a thermally stable silicon core surrounded by an organic-functionalized shell. The Si QDs exhibited exceptional performance in the adsorption remediation of textile wastewater. UV–Visible spectrophotometric monitoring showed rapid and effective removal of dye molecules, with absorbance-based color removal efficiencies reaching ~65% within 15 minutes and achieving up to ~95–96% under optimized contact times and adsorbent dosages. The enhanced adsorption efficiency is attributed to the high surface area, mesoporous structure, and abundance of reactive surface functional groups, which collectively promote strong interactions with dye molecules. These results highlight the synergistic effect of quantum confinement, surface functionalization, and porosity in enabling effective wastewater remediation.

In conclusion, the study establishes that waste-derived, Na–O functionalized Si QDs are structurally and optically well-defined nanomaterials with a crystalline core, functionalized surface, and excellent colloidal stability. Their wide bandgap, high surface area, and abundant surface functional groups enable efficient adsorption of textile dyes, demonstrating their potential as sustainable, low-cost, and environmentally friendly adsorbents. The findings support broader applications of such Si QDs in UV optoelectronics, photocatalysis, sensing, and bio-related technologies. It is recommended that future work explores the regeneration and reusability of the Si QDs in multiple adsorption cycles, optimization for industrial-scale wastewater treatment, and functional modifications to target specific classes of pollutants for enhanced environmental remediation.

5.0 References

Alizadehnoughabi, M., Elyassi, M., & Ashkani, O. (2025, December). *Developing quantum dots for new generation of water purification technologies, a mini review* [Paper presentation]. 14th International Conference on Materials Engineering & Metallurgy (IMAT 2025), Tehran, Iran.

Almomani, M. S., Ahmed, N. M., Rashid, M., Ibnaouf, K. H., Aldaghri, O. A., Madkhali, N., & Cabrera, H. (2022). Performance improvement of graded bandgap solar cell via optimization of energy levels alignment in Si quantum dot, TiO_2 nanoparticles, and porous Si. *Photonics*, 9, 11, 843. https://doi.org/10.3390/photonics 9110843

Bose, S., Ganayee, M. A., Mondal, B., Baidya, A., Chennu, S., Mohanty, J. S., & Pradeep, T. (2018). Synthesis of silicon nanoparticles from rice husk and their use as sustainable fluorophores for white light emission. *ACS Sustainable Chemistry &*

Engineering, 6, 5, pp. 6203–6210. https://doi.org/10.1021/acssuschemeng.7b04911

Chen, J., Yu, Y., Zhu, B., Han, J., Liu, C., Liu, C., Miao, L., & Fakudze, S. (2021). Synthesis of biocompatible and highly fluorescent N-doped silicon quantum dots from wheat straw and ionic liquids for heavy metal detection and cell imaging. *Science of the Total Environment, 765*, 142754. https://doi.org/10.1016/j.scitotenv.2020.142754

Chen, W., Yin, H., Cole, I., Houshyar, S., & Wang, L. (2024). Carbon dots derived from non-biomass waste: Methods, applications, and future perspectives. *Molecules, 29*(11), 2441. https://doi.org/10.3390/molecules29112441

Dhumal, P., Chakraborty, S., Ibrahim, B., Kaur, M., & Valsami-Jones, E. (2024). Green-synthesised carbon nanodots: A SWOT analysis for their safe and sustainable innovation. *Journal of Cleaner Production, 480*, 144115. https://doi.org/10.1016/j.jclepro.2024.144115

Eddy, N. O., Edet, U. E., Oladele J. O., Kelle, H. I., Ogoko. E. C., Odiongenyi, A. O., Ameh, P., Ukpe, R. A., Ogbodo, R., Garg, R. & Garg, R. (2023a). Synthesis and application of novel microporous framework of nanocomposite from trona for photocatalysed degradation of methyl orange dye. *Environmental Monitoring and Assessment*. DOI : 10.1007/s10661-023-12014-x.

Eddy, N. O., Garg, R., Garg, R., Garg, R., Ukpe, R. A. and Abugu, H. (2024c). Adsorption and photodegradation of organic contaminants by silver nanoparticles: isotherms, kinetics, and computational analysis. *Environ Monit Assess,* 196, 65, https://doi.org/10.1007/s10661-023-12194-6

Eddy, N. O., Jibrin, J. I., Ukpe, R. A., Odiongenyi, A., Iqbal, A., Kasiemobi, A. M., Oladele, J. O., & Runde, M. (2024a). Experimental and Theoretical Investigations of Photolytic and Photocatalysed Degradations of Crystal Violet Dye (CVD) in Water by oyster shells derived CaO nanoparticles (CaO-NP), *Journal of Hazardous Materials Advances,* 13, 100413, https://doi.org/10.1016/j.hazadv.2024.100413.

Eddy, N. O., Odiongenyi, A. O., Garg, R., Ukpe, R. A., Garg, R., El Nemir, A., Ngwu, C. M. and Okop, I. J. (2023b). Quantum and experimental investigation of the application of *Crassostrea gasar* (mangrove oyster) shell–based CaO nanoparticles as adsorbent and photocatalyst for the removal of procaine penicillin from aqueous solution. *Environmental Science and Pollution Research*, doi:10.1007/s11356-023-2686 8-8.

Eddy, N. O., Oladede, J., Eze, I. S., Garg, R., Garg, R., & Paktin, H. (2024b). Synthesis and characterization of CaO nanoparticles from periwinkle shell for the treatment of tetracycline-contaminated water by adsorption and photocatalyzed degradation. *Results in Engineering*, *103374*. https://doi.org/10.1016/j.rineng.2024.103374.

Esmaeili, Y., Toiserkani, F., Qazanfarzadeh, Z., Ghasemlou, M., Naebe, M., Barrow, C. J., Timms, W., & Jafarzadeh, S. (2025). Unlocking the potential of green-engineered carbon quantum dots for sustainable packaging biomedical applications and water purification. *Advances in Colloid and Interface Science*, *338*, 103414. https://doi.org/10.1016/j.cis.2025.103414.

Farirai, F., Ozonoh, M., Aniokete, T. C., Eterigho-Ikelegbe, O., Mupa, M., Zeyi, B., & Daramola, M. O. (2021). Methods of extracting silica and silicon from agricultural waste ashes and application of

the produced silicon in solar cells: A mini-review. *International Journal of Sustainable Engineering,* 14, 1, pp. 57–78. https://doi.org/10.1080/19397038.2020.1720854

Higuera, H., Zazueta-Raynaud, A., Heredia-Cancino, J. A., & Soto-B, M. A. (2024). Green synthesis of silicon quantum dots using *Ocimum basilicum* var. *purpurascens* as an organic reductor agent. *Silicon,* 16, 8, pp. 1–8. https://doi.org/10.1007/s12633-024-02948-3

Huo, X., He, Y., Ma, S., Jia, Y., Yu, J., Li, Y., & Cheng, Q. (2020). Green synthesis of carbon dots from grapefruit and its fluorescence enhancement. *Journal of Nanomaterials, 2020*, Article 8601307. https://doi.org/10.1155/2020/8601307

Kelle, H. I., Ogoko, E. C., Akintola O & Eddy, N. O. (2023). Quantum and experimental studies on the adsorption efficiency of oyster shell–based CaO nanoparticles (CaONPO) towards the removal of methylene blue dye (MBD) from aqueous solution. *Biomass Conversion and Biorefinery*, DOI : 10.1007/s13399-023-04947-7.

Moradialvand, Z., Parseghian, L., & Rajabi, H. R. (2025). Green synthesis of quantum dots: Synthetic methods, applications, and toxicity. *Journal of Hazardous Materials Advances, 18*, 100697. https://doi.org/10.1016/j.hazadv.2025.100697

Morozova, S., Alikina, M., Vinogradov, A., & Pagliaro, M. (2020). Silicon quantum dots: Synthesis, encapsulation, and application in light-emitting diodes. *Frontiers in Chemistry, 8*, 191. https://doi.org/10.3389/fchem.2020.00191

Nuhu, J. S., Awe, F. E., Garg, R., Garg, R., Eddy, N. O., & Paktin, H. (2025). Cobalt titanate nanocatalyst for enhanced photodegradation of atrazine: Kinetics, degradation efficiency, and mechanistic analysis. *BMC Chemistry, 19*, 31, https://doi.org/10.1186/s13065-025-01394-5.

Ogoko, E. C., Kelle, H. I., Akintola, O. & Eddy, N. O. (2023). Experimental and theoretical investigation of *Crassostrea* gigas (gigas) shells based CaO nanoparticles as a photocatalyst for the degradation of bromocresol green dye (BCGD) in an aqueous solution. *Biomass Conversion and Biorefinery*. https://doi.org/10.1007/s13399-023-03742-8.

Sachan, D., Ramesh, A., & Das, G. (2021). Green synthesis of silica nanoparticles from leaf biomass and its application to remove heavy metals from synthetic wastewater: A comparative analysis. *Environmental Nanotechnology, Monitoring & Management, 16*, 100467. https://doi.org/10.1016/j.enmm.2021.100467

Saito, K., Xu, T., & Ishikita, H. (2022). Correlation between C═O stretching vibrational frequency and pK_a shift of carboxylic acids. *The Journal of Physical Chemistry B*, *126*(27), 4999–5006. https://doi.org/10.1021/acs.jpcb.2c02193

Sarwat, S., Stapleton, F., Willcox, M. D. P., O'Mara, P. B., & Roy, M. (2025). Hydrophobic Silicon Quantum Dots for Potential Imaging of Tear Film Lipid Layer. *Nanomaterials*, *15, 7,* 552. https://doi.org/10.3390/nano15070552.

Srinivasan, G., Hoey, J., Anderson, K. J., Frohlich, M. T., Krishnan, R., Sivaguru, J., Sibi, M. P., & Boudjouk, P. (2016). Synthesis of silicon quantum dots using cyclohexasilane (Si_6H_{12}). *Journal of Materials Chemistry C,* 4, 35, pp. 8234–8238, https://doi.org/10.1039/C6TC01435F

Wu, J., Dai, J., Shao, Y., & Sun, Y. (2015). One-step synthesis of fluorescent silicon quantum dots (Si-QDs) and their application for cell imaging. *RSC*

Advances, *5*(102), 83581–83587. https://doi.org/10.1039/C5RA13119G

Xiao, Z., Fan, N., Zhu, W., Qian, H.-L., Yan, X.-P., Wang, Z., & Rasmann, S. (2023). Silicon nanodots increase plant resistance against herbivores by simultaneously activating physical and chemical defenses. *ACS Nano,* *17*(3), 3107–3118. https://doi.org/10.1021/acsnano.2c12070

Yu, J., Bian, Y., *W*ang, R., Zhou, S., Wang, Z., Wang, D., & Li, H. (2024). Coconut shell carbon preparation for Rhodamine B adsorption and mechanism study. *Molecules*, *29, 17,* 4262. https://doi.org/10.3390/molecules29174262.

Zhang, Z., Wei, C., Ma, W., Li, J., Xiao, X., & Zhao, D. (2019). One-step hydrothermal synthesis of yellow and green emitting silicon quantum dots with synergistic effect. *Nanomaterials, 9, 3,* 466. https://doi.org/10.3390/nano9030466.

Declaration

Funding sources

No funding

Competing Statement: Financial Interests Statement:

There are no competing financial interests in this research work.

Ethical considerations

Not applicable

Data availability

The microcontroller source code and any other information can be obtained from the corresponding author via email.

Author Contributions

ECO conceived the study, carried out the synthesis and characterization of the silicon quantum dots, analyzed data, and drafted the manuscript. HIK contributed to experimental design, optical and spectroscopic analyses, and data interpretation. AHA handled wastewater sampling, adsorption experiments, and environmental analysis. NOE supervised the research, refined the methodology, critically reviewed the manuscript, and provided overall scientific guidance.